H2Av FACILITATES H3S10 PHOSPHORYLATION BUT IS NOT REQUIRED FOR HEAT SHOCK-INDUCED CHROMATIN DECONDENSATION OR TRANSCRIPTIONAL ELONGATION

Yeran Li, Chao Wang, Weili Cai, Saheli Sengupta, Michael Zavortink, Huai Deng, Jack Girton, Jørgen Johansen and Kristen M. Johansen

Roy J. Carver Department of Biochemistry, Biophysics, and Molecular Biology
Iowa State University
Ames, Iowa 50011

Key words: *JIL-1 kinase, chromatin structure, histone H3S10 phosphorylation, Drosophila, H2Av*

Summary statement: *We have revisited the roles of H2Av and the JIL-1 kinase in chromatin decondensation associated with transcriptional activation and show that they are not required contrary to current reports.*

CORRESPONDENCE:

Kristen M. Johansen and Jørgen Johansen
Roy J. Carver Department of Biochemistry, Biophysics, and Molecular Biology
Iowa State University
Ames, Iowa 50011
E-mail: *kristen@iastate.edu; jorgen@iastate.edu*

ABSTRACT

A model has been proposed where JIL-1 kinase-mediated H3S10 and H2Av phosphorylation is required for transcriptional elongation and heat shock-induced chromatin decondensation to occur. However, here we show that while H3S10 phosphorylation is indeed compromised in the *H2Av* null mutant we find that chromatin decondensation at heat shock loci is unaffected both in the absence of JIL-1 as well as of H2Av and that there is no discernable decrease in the elongating form of Pol II in either mutant. Furthermore, mRNA for the major heat shock protein Hsp70 is transcribed at robust levels in both *H2Av* and *JIL-1* null mutants. Using a different chromatin remodeling paradigm that is JIL-1 dependent we provide evidence that ectopic tethering of JIL-1 and subsequent H3S10 phosphorylation recruits PARP-1 to the remodeling site independently of H2Av phosphorylation. Thus these data strongly suggest that H2Av or H3S10 phosphorylation by JIL-1 is not required for chromatin decondensation or transcriptional elongation in *Drosophila*.

INTRODUCTION

The JIL-1 kinase localizes specifically to euchromatic interband regions of polytene chromosomes and is the kinase responsible for histone H3S10 phosphorylation at interphase in *Drosophila* (Jin et al., 1999; Wang et al., 2001). Furthermore, JIL-1 is enriched about two-fold on the male X chromosome and implicated in transcriptional regulation as well as dosage compensation (Jin et al., 1999; Lerach et al., 2005, 2006). In a recent study Cai et al. (2014) determined the genome-wide relationship of JIL-1 kinase-mediated H3S10 phosphorylation with gene expression and the distribution of the epigenetic H3K9me2 mark. The results showed that the H3S10ph mark in wild-type salivary gland cells is predominantly enriched at active genes whereas the H3K9me2 mark largely is associated with inactive genes. However, mutation in *JIL-1* resulted in 2-fold or greater changes of salivary gland expression in 1539 genes with approximately half showing increased expression while the other half were down-regulated. Notably, H3K9me2 marking also changed and was inversely correlated with expression level: genes showing decreased expression in the mutant were found to have acquired the H3K9me2 mark while genes showing increased expression had either no or reduced levels of H3K9me2 marking as compared to wild-type. These results are consistent with a model where the H3S10ph mark itself is not essential for gene transcription but rather that gene expression levels are modulated by the levels of the H3K9me2 mark independently of the state of the H3S10ph mark (Wang et al., 2011a: 2011b; 2012; Girton et al., 2013; Cai et al., 2014). Thus, H3S10 phosphorylation acts indirectly to maintain active transcription by counteracting H3K9 dimethylation and gene silencing. Recently, partly based on the finding that H3S10 phosphorylation is impaired in the absence of the H2Av histone variant an alternative model has been proposed in which JIL-1 is required for gene expression by activating poly(ADP-ribose) polymerase 1 (PARP-1) through phosphorylation of the COOH-terminus of H2Av (Thomas et al., 2014). In the model this leads to loosening of nucleosome structure allowing for subsequent

H3S10 phosphorylation by JIL-1 that is required for transcription by the RNA polymerase II (Pol II) machinery to occur (Thomas et al., 2014; Ivaldi et al., 2007). Particularly, Thomas et al. (2014) claim that JIL-1 kinase activity is required for transcriptional elongation during the heat-shock response as well as for PARP-1 dependent chromatin decondensation (puffing) at heat shock loci. Since these results are incompatible with those of Cai et al. (2014) described above and the demonstration by Cai et al. (2008) that JIL-1 is not enriched at developmental or heat shock-induced polytene chromosome puffs, in this study we reexamined some of the key findings of Thomas et al. (2014). While our results confirm that H3S10 phosphorylation is indeed compromised in the *H2Av* null mutant we find that chromatin decondensation at heat shock loci is unaffected both in the absence of JIL-1 as well as of H2Av and that there is no discernable decrease in the elongating form of Pol II in either mutant. These results along with our previous studies (Deng et al. 2007; 2008; Cai et al., 2008; 2014; Wang et al., 2011a; 2011b; 2012) provide further evidence that redistribution of the epigenetic H3K9me2 mark that occurs in the absence of H3S10 phosphorylation leads to transcriptional defects and argue against the model of Thomas et al. (2014) and Ivaldi et al. (2007) that JIL-1 mediated H3S10 phosphorylation is required for Pol II dependent transcription to occur. Furthermore, in a different chromatin decondensation paradigm that is JIL-1 dependent (Deng et al., 2008; Li et al., 2013; Wang et al., 2013) we provide evidence that ectopic tethering of JIL-1 and subsequent H3S10 phosphorylation recruits PARP-1 to the remodeling site independently of H2Av and H2Av phosphorylation.

RESULTS

Jil-1 kinase localizes to chromatin in *H2Av* null mutants at wild-type levels but euchromatic H3S10 phosphorylation is decreased

Thomas et al. (2014) reported that JIL-1 co-localizes with H2Av and that H3S10 phosphorylation is completely absent in *H2Av* null mutant larvae ($H2Av^{810}/H2Av^{810}$) (Van Daal and Elgin, 1992). To verify these claims we performed double labelings of polytene squash preparations with antibodies to JIL-1 and H2Av. As illustrated in Fig. 1A we found that while H2Av and JIL-1 do co-localize at many locations as indicated by yellow/orange coloring, this co-localization was not universal as many interband locations were only positive for either JIL-1 or H2Av. This distribution is similar to that shown in Fig. 2B of Thomas et al. (2014). However, although JIL-1 and H2Av do not show complete co-localization, H3S10 phosphorylation was greatly diminished throughout the chromosome arms in *H2Av* null polytene chromosomes (Fig. 1B). Interestingly, the H3S10 phosphorylation by JIL-1 associated with the H3S10phK9me2 composite mark on pericentric heterochromatin and on the fourth chromosome (Wang et al., 2014) was unaffected (Fig.1B and 1C). Figure 1D shows that the H3K9me2 mark spreads to ectopic locations on the chromosome arms in the *H2Av* null mutant background as predicted by the decrease in euchromatic H3S10 phosphorylation (Zhang et al., 2006). Furthermore, JIL-1 antibody labelings and immunoblotting of salivary gland protein extracts show that JIL-1 is localized to chromatin (Figs. 1B and 1D) and present at wild-type levels in the *H2Av* null mutant although H3S10ph levels are substantially reduced (Fig. 1E). In order to quantify this reduction we determined the H3S10ph levels on immunoblots of salivary gland protein extracts from *H2Av* mutant larvae as a percentage relative to the levels in wild-type larvae. The data from six independent biological replicates indicate that the average reduction was about 5-fold (19.8±7.2%, n=6). Moreover, the immunoblot indicates that H3K9me2 levels are indistinguishable from wild-type levels in the *H2Av* null mutant as well (Fig. 1E). This result is contrary to that of Swaminathan et al. (2005) who reported that H3K9me2

is not present in *H2Av* null mutants. However, we confirm the finding of Thomas et al. (2014) that H3S10ph levels are reduced at euchromatic sites in *H2Av* null mutants. Furthermore we show that this reduction occurs despite that JIL-1 protein levels are unaffected and that JIL-1 localizes to chromatin in the absence of H2Av.

In order to verify that changes to H3S10 phosphorylation in the $H2Av^{810}$ homozygous mutant was caused by the absence of H2Av we expressed a *H2Av-RFP* transgene (Deng et al., 2005) in the mutant. As illustrated in Figs. 2A and 2B this restored H3S10ph to wild-type levels indicating rescue of H2Av function. We also expressed a *JIL-1-GFP* transgene under heat shock promoter control (Jin et al., 1999) in the *H2Av* null mutant background. Interestingly, overexpressing JIL-1 substantially restored H3S10 phosphorylation levels as indicated by both the immunofluorescence in polytene chromosome squash preparations (Fig. 2C) as well as by immunoblot analysis (Fig. 2D). This suggests that H2Av is not required for JIL-1 H3S10 phosphorylation but rather facilitates JIL-1 kinase activity when both proteins are present at wild-type levels.

H2Av phosphorylation at S137 is indistinguishable from wild-type in *JIL-1* null mutants in vivo.

A key feature of the model of Thomas et al. (2014) is that phosphorylation of H2AvS137 (H2Avph) by JIL-1 is required for chromatin decondensation and subsequent H3S10 phosphorylation. However, this conjecture is mainly based on in vitro phosphorylation assays (Thomas et al., 2014) and kinases are well known for promiscuity in such assays (Peck, 2006; Mohamed and Hollfelder, 2012; Xue et al., 2012). We therefore examined H2Av and H2Avph levels in wild type and *JIL-1* null ($JIL\text{-}1^{z2}/JIL\text{-}1^{z2}$) mutant chromosome squash preparations as well as on immunoblots of protein extracts from salivary glands (Fig. 3). For H2Avph labeling we used a previously validated mAb raised specifically to the *Drosophila* phosphorylated H2AvS137 residue (Lake et al., 2013). Since chromosome morphology is grossly perturbed in the *JIL-1* null

mutant (Deng et al., 2005) we expressed a CFP-tagged JIL-1 COOH-terminal construct (JIL-1-CTD) in the *JIL-1* null mutant background that rescues chromosome morphology to near wild-type without JIL-1 kinase activity (Bao et al., 2008). This allows for easier comparisons of mutant squash preparations with those of wild-type (Wang et al., 2013). We found that H2Av and H2Avph distribution in *JIL-1* mutants was indistinguishable from that of wild-type polytene squash preparations (Fig. 3A) as were the levels of H2Av (Fig. 3B) and H2Avph (Fig. 3C). As a control H2Av and H2Avph antibody labeling was undetectable or at very low levels in the *H2Av* null mutant background (Fig. 3A-C). Thus, these results indicate that JIL-1 is not a major, if at all, kinase for H2AvS137 phosphorylation in vivo.

Decreased levels of PARP-1 activity does not affect H3S10 phosphorylation by JIL-1

In the model of Thomas et al. (2014) PARP-1 activation following H2Av phosphorylation by JIL-1 leads to loosening of chromatin structure allowing for JIL-1 mediated H3S10 phosphorylation to occur. A prediction of this model is that H3S10 phosphorylation would be expected to be decreased in mutants with reduced PARP-1 activity. In order to test this we examined H3S10ph levels and distribution in $Parp^{C03256}$ homozygous salivary glands (Fig. 4). $Parp^{C03256}$ is a strong hypomorphic allele with only low levels of residual poly(ADP ribosyl)ation activity (Kotova et al., 2010). As illustrated in Fig. 4A the distribution and levels of H3S10ph are indistinguishable in wild type and $Parp^{C03256}$ homozygous mutant polytene chromosome squash preparations. That the levels of H3S10ph were undiminished in the $Parp^{C03256}$ homozygous mutant compared to wild type was confirmed by immunoblotting (Fig. 4B). Thus, these results suggest that PARP-1 activity and poly(ADP ribosyl)ation are not required for JIL-1 mediated H3S10 phosphorylation.

Neither JIL-1 nor H2Av is required for chromatin decondensation or transcriptional elongation during heat shock

Thomas et al. (2014) reported that chromatin decondensation and transcriptional elongation during the heat shock response requires JIL-1 and H2Av phosphorylation. However, in a *Su(var)3-9* mutant with reduced H3K9 HMTase activity, chromosome defects and the lethality associated with the *JIL-1* null phenotype are substantially rescued (Deng et al., 2007). Furthermore, comparing global transcription profiles from wild type and *JIL-1* null mutant salivary glands Cai et al. (2014) found that overall levels of transcription were unchanged with about half of changed genes upregulated and the other half downregulated. This indicates that Pol II transcription can occur even in the complete absence of JIL-1 kinase activity and its associated loss of interphase H3S10 phosphorylation. As well, we have previously shown that transcription of heat shock loci still occurs in the null *JIL-1* mutant background (Cai et al., 2008). In order to reaffirm the previous observation that loss of JIL-1 reduced but did not eliminate heat-shock-induced transcription as well as compare this effect with results observed after loss of H2Av, we investigated the distribution of Pol II0^{ser2} and Pol II0^{ser5} labeling and measured heat shock transcript levels in both *JIL-1* null and in *H2Av* null mutant backgrounds (Fig. 5). The antibody to Pol II0^{ser2} recognizes the elongating form of RNA polymerase II, which is phosphorylated at Ser2 in the COOH-terminal domain and which serves as a marker for active transcription, whereas antibody to Pol II0^{ser5} recognizes the paused form (Weeks et al., 1993; Boehm et al., 2003; Ivaldi et al., 2007). Figure 5A shows labeling of heat shock puffs by Pol II0^{ser2} and Pol II0^{ser5} antibodies in polytene chromosome squashes from wt, *H2Av* null, *JIL-1* null, and a *JIL-1* null expressing the JIL-1-CTD only (in order to restore chromosome morphology) salivary glands. In all mutant genotypes there was robust labeling of heat shock puffs indistinguishable from wild-type. To quantify this aspect we measured the area of the 87A/C heat shock puffs labeled by Pol II0

antibody and normalized it to the width of the adjacent un-puffed region in order to adjust for different degrees of chromosome spreading during the squash process. As illustrated by the box plot in Fig. 5B there was no statistical difference ($P > 0.15$, ANOVA test) between the normalized puff size from the various genotypes and wild type. Measurements were obtained from more than 30 salivary gland nuclei from at least five different larvae for each genotype. In addition, we determined the number of nuclei with clearly recognizable puffs among the total number of nuclei examined and found a frequency close to 70% for all the genotypes (Fig. 5C). Furthermore, on immunoblots of extracts from wt, *H2Av* null, *JIL-1* null, and JIL-1-CTD expressing *JIL-1* null salivary glands there was no detectable difference in Pol II0^{ser2} or Pol II0^{ser5} levels (Fig. 5D).

These results indicate that the Pol II complex is transcriptionally active in both *JIL-1* and *H2Av* null mutant backgrounds. However, in order to obtain a more direct measure of the level of heat shock gene transcription, we performed quantitative RT-PCR assays on the six nearly identical genes at Hsp70, the major heat shock protein in *Drosophila* (Gong and Golic, 2004) before or after heat shock in the *H2Av* null mutant background and compared the results with those obtained from the *JIL-1* null mutant background. In the experiments qRT-PCR results from primers that amplify transcripts from all six *hsp70* genes were normalized to qRT-PCR results from a primer pair specific to the non-heat shock sensitive Rp49 ribosomal protein as in Cai et al. (2008). Three independent experiments with total RNA isolated from wt, *H2Av* null, and *JIL-1* null third instar larvae were performed; in each case qRT-PCR determination of transcript levels was performed in duplicate. As illustrated in Fig. 5E, very low levels of *hsp70* mRNA transcripts in wild type, *JIL-1* and *H2Av* mutant backgrounds were detected under non-heat shock conditions. However, a robust increase in *hsp70* mRNA transcript levels was detected in response to heat shock treatment in all three genotypes relative to *rp49* transcript levels (Fig. 5E). The increase in *JIL-1* and *H2Av* null mutant larvae was at least two orders of magnitude larger than under non-heat shock conditions. Thus, although total transcript levels were reduced (1/3 to 2/3) compared to wild-type, a strong heat shock response was clearly observed. The results shown in Fig. 5E for

transcript levels in the *JIL-1* null mutant background replicate and reaffirm the previous findings in Fig. 8C of Cai et al. (2008).

PARP-1, but neither H2Av nor H2Avph is upregulated at LacI-JIL-1 targeting sites

Previously, we showed that ectopic tethering of LacI-JIL-1 to *lacO* repeats inserted into a condensed, heterochromatic-like polytene chromosome band resulted in robust H3S10 phosphorylation and a more open euchromatic state at the targeting region (Deng et al., 2008). LacI tethering affords an excellent experimental system to assess whether targeting of JIL-1 could induce H2Av phosphorylation and/or recruitment of H2Av to the targeting site. As illustrated in Fig. 6A tethering of LacI-JIL-1 to 96C1-2 resulted in band-"opening" as previously reported (Deng et al., 2008). However, labeling of the insertion site with H2Av and H2Avph antibody (Fig. 6A), respectively, revealed no signal above background levels suggesting no direct involvement of H2Av or H2Av phosphorylation in this process. For comparison, Fig. 6B shows control anti-H2Av and anti-H2Avph antibody labelings when LacI-GFP was tethered instead of LacI-JIL-1. In contrast to LacI-JIL-1 tethering of LacI-GFP induced no opening of the band and both H2Av and H2Avph antibody-labeling were coinsiding with the targeting site. In order to further exclude a role for H2Av in this chromation remodeling we tethered LacI-JIL-1 to the targeting site in a homozygous $H2Av^{810}$ null mutant background. As illustrated in Fig. 6C this resulted in robust H3S10 phosphorylation at the targeting site and "opening" of the band. However, to examine the possible involvement of PARP-1, in the absence of a suitable antibody to *Drosophila* PARP-1, we expressed a GFP-tagged PARP-1 construct (Parp-GFP) (Tulin et al., 2002) together with LacI-JIL-1. Interestingly, as shown in Fig. 6D Parp-GFP accumulates at the LacI-JIL-1 targeting site suggesting a possible role for PARP-1 in the chromatin remodeling process. To investigate whether the recruitment was caused by direct interactions between JIL-1 and PARP-1 or whether it was dependent on phosphorylation of H3S10 we expressed a LacI-tagged "kinase dead" and two deletion constructs (CTD and ΔCTD) in a *JIL-1* null background as previously described (Deng et al., 2008; Li et al., 2013). JIL-1 can be divided into four main domains including an

amino-terminal domain (NTD), two kinase domains (KDI and KDII), and a carboxy-terminal domain (CTD) (Jin et al., 1999). The CTD-domain of JIL-1 is without kinase activity but sufficient for proper chromatin localization (Deng et al., 2005; Bao et al., 2008), whereas the ΔCTD JIL-1 construct without the CTD-domain has kinase activity for histone H3S10 despite that it does not localize properly (Bao et al., 2008; Wang et al., 2011b). Figure 7 shows "smush" preparations in which these constructs were co-expressed with Parp-GFP. The smush preparation is a modified whole-mount staining technique where nuclei from dissected salivary glands are gently compressed beneath a coverslip to flatten them before fixation (Wang et al., 2001; Cai et al., 2008). As indicated by the white arrows (Fig. 7) only constructs with H3S10 phosphorylation activity (FL and ΔCTD) recruit Parp-GFP to the targeting site, whereas the 'kinase dead" construct, which only differs from wild-type JIL-1 at two alanine mutations in the two catalytic domains, does not. Taken together these findings indicate that PARP-1 correlates with JIL-1 induced chromatin remodeling sites and H3S10 phosphorylation independently of H2Av and H2Av phosphorylation in this paradigm.

DISCUSSION

In this study we have revisited the roles of H2Av and the JIL-1 kinase in chromatin decondensation associated with transcriptional activation especially during the heat shock response. We provide evidence that heat shock induced chromatin puffs occur both in *H2Av* and *JIL-1* null mutant backgrounds and that the size and frequency of such puffs are indistinguishable from wild-type. Furthermore, we show that heat shock puffs in *JIL-1* and *H2Av* null mutant backgrounds are strongly labeled by Pol II0^{ser2} antibody indicating that Pol II0^{ser2} is actively involved in heat shock induced transcription in the absence of H2Av as well as of JIL-1 kinase activity. These findings were corroborated by immunoblot analysis that showed that both Pol II0^{ser2} and Pol II0^{ser5} levels were unchanged in these mutants compared to wild type as also previously demonstrated by Cai et al. (2008). Quantitative RT-PCR assays revealed that Hsp70 mRNA is transcribed at robust levels in *H2Av* and *JIL-1* null mutants, confirming the results of Cai et al. (2008). Thus these data strongly suggest that H2Av and histone H3S10 phosphorylation by JIL-1 is not required for heat shock-induced chromatin decondensation or transcriptional elongation in *Drosophila*. Moreover, we found that H2Av phosphorylation in vivo was indistinguishable from wild type in the absence of JIL-1 and that H3S10ph levels were unaffected in mutants with greatly reduced PARP-1 activity. These results are contrary to the model and many of the findings of Thomas et al. (2014). We cannot explain the discrepancies apart from that they may be caused by technical issues such as the use of whole larval extracts containing a substantial mitotic H3S10ph component (Wang et al., 2001; Cai et al., 2008) and use of hypomorphic instead of null *JIL-1* alleles. Instead, the conclusions of the present study are consistent with a number of previous reports showing that polytene chromosome immunodetection of JIL-1 and H3S10ph shows no to minimal overlap with either Pol II0^{ser5} (paused) or Pol II0^{ser2} (elongating) Pol II labeling (Cai et al., 2008; Regnard et al., 2011; Wang et al., 2013). The present results are also consistent with

previous studies that did not detect any JIL-1 or H3S10ph signal associated with developmental or heat shock-induced puffs (Cai et al., 2008).

The finding that heat shock protein transcription levels were attenuated somewhat in *JIL-1* and *H2Av* mutant backgrounds, although two orders of magnitudes larger than under non-heat shock conditions, is directly compatible with the model of Cai et al. (2014) that such decreases are caused by the redistribution of the H3K9me2 silencing mark modulating gene transcription that occurs in the absence of H3S10 phosphorylation (Wang et al., 2012b; 2013). This hypothesis is further supported by our demonstration in the present paper that H3K9me2 spreads to the chromosome arms and that H3K9me2 levels are indistinguishable from wild type in the *H2Av* null mutant.

However, our data do confirm the finding of Thomas et al. (2014) that euchromatic H3S10ph levels are severely reduced in the absence of H2Av although pericentric and 4th chromosome H3S10 phosphorylation is unaffected. Furthermore we show that JIL-1 is present at wild-type levels in the *H2Av* null mutant and that it binds to chromatin. Thus, the reduced levels of H3S10ph on the euchromatic chromosome arms is not a consequence of JIL-1 degradation, as is the case in the absence of Mof acetyltransferase activity in males (Li et al., 2012), or of a failure of JIL-1 to localize to chromatin, possibilities not addressed by Thomas et al. (2014). Rather, these findings suggest a model where JIL-1 H3S10 phosphorylation is facilitated by a direct interaction of JIL-1 with H2Av in a complex providing an optimal conformation for JIL-1 enzymatic activity. In this scenario without H2Av JIL-1 mediated H3S10 phosphorylation is less efficient leading to reduced levels. Alternatively, H2Av dependent changes to nucleosome structure and histone tail alignment could serve the same function. That H2Av is not *required* for H3S10 phosphorylation by JIL-1 is further supported by the finding that overexpressing JIL-1 in the *H2Av* null mutant substantially restores H3S10ph levels.

In this study we also examined the roles of H2Av, H2Avph, and PARP-1 in a different chromatin decondensation paradigm from that of heat shock induced chromosome puffs that is

JIL-1 dependent. In this paradigm ectopic targeting of JIL-1 using a LacI-tethering system induces robust histone H3S10 phosphorylation and a change in higher order chromatin structure from a condensed heterochromatic-like state to a more open euchromatic state (Deng et al., 2008). However, as was the case for heat shock-induced chromatin decondensation we found no evidence for a direct involvement of H2Av or H2Avph in this process. Rather, the results suggested that PARP-1 was recruited to the chromatin remodeling site by H3S10 phosphorylation itself, independently of any structural contributions from the JIL-1 protein. Thus, these data suggest a possible role for PARP-1 in chromatin remodeling downstream, not upstream (Thomas et al., 2014), of JIL-1-mediated H3S10 phosphorylation. It will be of interest in future studies to further define PARP-1's role and the mechanisms of chromatin decondensation caused by H3S10 phosphorylation.

MATERIALS AND METHODS

Drosophila melanogaster stocks

Drosophila lines were grown at 25°C according to standard methods (Roberts, 1998); Canton S was used for wild type preparations. The *JIL-1*^{z2} null allele is from Wang et al. (2001) and Zhang et al. (2003); the *H2Av*^{810} null allele is described in Van Daal and Elgin (1992), and the *Parp*^{C03256} hypomorphic allele in Ji and Tulin (2009). LacI-tagged JIL-1 constructs were generated and described in Deng et al. (2008) and Li et al. (2013). These lines include: LacI-JIL-1-FL, LacI-JIL-1-CTD, LacI-JIL-1-ΔCTD, and LacI-JIL-1-"kinase-dead". GAL4-expression was driven by generating recombinant lines with *Sgs3-GAL4* and *da-GAL4* drivers obtained from the Bloomington Stock Center. Recombinant *JIL-1*^{z2}, *da-GAL4* and *H2Av*^{810}, *Sgs3-GAL4* chromosomes were generated as described by Ji et al. (2005). Deng et al. (2008) and Li et al. (2013) describe the Lac operator insertion line *P11.3*. Bao et al. (2008) generated the CFP-tagged JIL-1-CTD construct. S. Heidmann provided the *H2AvDmRFP1* transgenic line which has been previously described (Deng et al., 2005). Jin et al. (1999) described the *hsp83* promoter-driven full-length JIL-1-GFP transgenic line *GF29.1.* The Parp-GFP transgenic fly line was the gift of Dr. A. Tulin and is described in Tulin et al. (2002). Balancer chromosomes and markers are described in Lindsley and Zimm (2012). Heat shock experiments followed the protocols of Nowak et al. (2003) and Cai et al. (2008) with wandering third instar larvae subjected to 25 min of heat shock treatment at 37°C.

Immunohistochemistry

Wang et al., (2001) described the salivary gland nuclei smush preparations and standard polytene chromosome squash preparations followed the methods of Cai et al. (2010). Antibody labeling protocols were as in Johansen and Johansen (2003) and Johansen et al. (2009). Primary antibodies used in this study include rabbit anti-H3S10ph (Epitomics, 1173-1, RRID:AB_732930

and Cell Signaling, #9701, RRID:AB_331535), mouse anti-H3K9me2 (Abcam, 1220, RRID:AB_449854), rabbit anti-JIL-1 (Jin et al., 1999), chicken anti-JIL-1 (Jin et al., 2000), mouse anti-Pol II0^{Ser2} (BioLegend, 920204 RRID:AB_2616695), mouse anti-Pol II0^{Ser5} (Covance, MMS-134R, RRID:AB_10119940), mouse anti-tubulin (Sigma-Aldrich, T9026, RRID:AB_477593), mouse anti-H2Av was provided by Dr. R. Glaser and has been previously characterized (Madigan et al., 2012), mouse anti-H2Avph (RRID:AB_2618077) (Lake et al., 2013) obtained from the Developmental Studies Hybridoma Bank, mouse anti-Lamin Dm_0 mAb HL1203 was provided by Drs. M. Paddy and H. Saumweber and has been previously characterized (Gruenbaum et al., 1988), chicken anti-GFP (Aves Labs, GFP-1020, RRID:AB_10000240), Mouse anti-LacI (Millipore, 05-503, RRID:AB_11211192), mouse anti-H3S10phK9me2 (Millipore, 05-1354, RRID:AB_11212491), and rabbit anti-H3 (Cell Signaling, 9715, RRID:AB_331563). DNA was visualized by staining with Hoechst 33258 (Molecular Probes) in PBS. The appropriate species- and isotype- specific Texas Red-, TRITC-, and FITC-conjugated secondary antibodies (Cappel/ICN, Southern Biotech) were used (1:200 dilution) to visualize primary antibody labeling. Mounting of the preparations were in 90% glycerol including 0.5% n-propyl gallate. Epifluorescence optics were used to examine the preparations on a Zeiss Axioskop microscope. Images were obtained and digitized using a Spot CCD camera. A Leica confocal TCS SP5 tandem scanning microscope system equipped with separate Argon-UV, Argon, and Krypton lasers and the appropriate filter sets for Hoechst, FITC, Texas Red and TRITC imaging was used. A Plan-Apochromat 63x/1.4 oil objective was used to obtain a separate series of confocal images for each fluorophor of double-labeled preparations. Images were obtained simultaneously with z-intervals of approximately 0.5 µm. Photoshop (Adobe) was used to pseudocolor, image process, and merge images. Non-linear adjustments were performed for some images of Hoechst labeling for the best chromosomal visualization.

Immunoblot analysis

Protein extractions from third instar larval salivary glands (homogenization buffer: 20 mM Tris-HCl pH 8.0, 150 mM NaCl, 10 mM EDTA, 1 mM EGTA, 0.2% Triton X-100, 0.2% NP-40, 2 mM Na_3VO_4, 1 mM PMSF, 1.5 µg/ml aprotinin) were separated by SDS-PAGE and immunoblotted (Sambrook and Russell, 2001) using the Bio-Rad Mini PROTEAN III system and 0.2 µm nitrocellulose. Anti-mouse, anti-chicken or anti-rabbit HRP-conjugated secondary antibody (Bio-Rad) (1:3000) was used to detect primary antibody using a ChemiDoc-It®TS2 Imager (UVP, LCC). Digital images were analyzed using the NIH-ImageJ software to quantify the immunolabeling as previously described (Wang et al., 2001). ImageJ's gel analysis feature was used to determine the average pixel value after the grayscale exposure of the images was adjusted so only a few pixels in the wild type lanes were saturated. Levels in *H2Av* mutant larvae were determined as a percentage relative to the level determined for wild type control larvae after normalization to the tubulin loading control lanes.

Analysis of gene expression by qRT-PCR

The MicroPoly(A)Purist Small-Scale mRNA Purification Kit (Ambion) was used to extract total RNA from 10 pooled whole third instar larvae of each genotype [wild type, *JIL-1*^{z2}/*JIL-1*^{z2}, *H2Av*^{810}/*H2Av*^{810}, and *JIL-1-CTD; JIL-1*^{z2}*, da-GAL4/JIL-1-1*^{z2}] after heat shock; the same was done for non-heat shock controls. SuperScript III Reverse Transcriptase (Invitrogen) was used to make cDNA from this RNA that was then used as template for quantitative real-time (qRT) PCR using a Stratagene Mx4000 real-time cycler. PCR reactions included Brilliant II SYBR Green QPCR Master Mix (Stratagene) and the corresponding primers: *rp49*, 5′-AACGTTTACAAATGTGTATTCCGACC-3′ and 5′-ATGACCATCCGCCCAGCATACAGG-3′; *Hsp70*, 5′-GTCATCACAGTTCCAGCCTACTTCAAC-3′ and 5′-CTGGGTTGATGGATAGGTTGAGGTTC-3′. A 10 min 95˚C denaturation step was followed by 40 cycles of 30 s at 95°C, 60 s at 59°C, and 40 s at 72°C. The Stratagene algorithm was used to plot

fluorescence intensities against the number of cycles and a calibration curve based on dilution of concentrated cDNA was used to quantify mRNA levels; *rp49* results were used for normalization.

Heat shock puff size and frequency

Heat shock puffs as well as adjacent areas of chromosomes in digital images from third instar polytene squash preparations labeled with RNA Pol II0^{ser2} or Pol II0^{ser5} antibody were outlined using ImageJ and with the outlined area determined in square pixels. Subsequently heat shock puff areas were normalized as the ratio of the area of the puff to the width of the adjacent chromosome bands. The frequency of puff appearances was determined as the number of nuclei with clearly recognizable puffs divided by the total number of nuclei examined. Box plot and stacking plots were made using R (v3.0.1).

ACKNOWLEDGMENTS

We thank members of the laboratory for discussion, advice, and critical reading of the manuscript. We especially thank Drs. S. Heidman, A. Tulin, R. Glaser, H. Saumweber, and M. Paddy for fly stocks and reagents.

COMPETETING INTERESTS

The authors declare no competing or financial interests.

AUTHOR CONTRIBUTIONS

Contributed to editing the manuscript: YL CW WC SS MZ HD JG JJ KMJ. Conceived and designed the experiments: KMJ JJ JG. Performed the experiments: YL CW WC SS MZ HD. Analyzed the data: YL CW WC SS MZ HD JG JJ KMJ. Wrote the paper: JJ KMJ.

FUNDING

This work was supported by NIH Grant GM062916 (KMJ/JJ).

REFERENCES

Bao, X., Cai, W., Deng, H., Zhang, W., Krencik, R., Girton, J., and Johansen, K.M. (2008). The COOH-terminal domain of the JIL-1 histone H3S10 kinase interacts with histone H3 and is required for correct targeting to chromatin. *J. Biol. Chem.* **283***,* 32741-32750.

Boehm, A.K, Saunders, A., Werner, J., and Lis, J.T. (2003). Transcription factor and polymerase recruitment, modification, and movement on *dhsp70* in vivo in the minutes following heat shock. *Mol. Cell. Biol.* **23,** 7628-7637.

Cai, W., Bao, X., Deng, H., Jin, Y., Girton, J., Johansen, J., and Johansen, K.M. (2008). RNA polymerase II-mediated transcription at active loci does not require histone H3S10 phosphorylation in *Drosophila*. *Development* **135,** 2917-2925.

Cai, W., Jin, Y., Girton, J., Johansen, J., and Johansen, K.M. (2010). Preparation of polytene chromosome squashes for antibody labeling. *J. Vis. Exp.* http://www.jove.com/index/Details.stp?ID=1748.

Cai, W., Wang, C., Li, Y., Yao, C., Shen, L., Liu, S., Bao, X., Schnable, P., Girton, J., Johansen, J., and Johansen, K.M. (2014). Genome-wide analysis of regulation of gene expression and H3K9me2 distribution by JIL-1 mediated histone H3S10 phosphorylation in *Drosophila*. *Nucleic Acids Res.* **42,** 5456-5467.

Deng, H., Zhang, W., Bao, X., Martin, J.N., Girton, J., Johansen, J., and Johansen, K.M. (2005). The JIL-1 kinase regulates the structure of *Drosophila* polytene chromosomes. *Chromosoma* **114,** 173-182.

Deng, H., Bao, X., Zhang, W., Girton, J., Johansen, J., and Johansen, K.M. (2007). Reduced levels of Su(var)3-9 but not Su(var)2-5 (HP1) counteract the effects on chromatin structure and viability in loss-of-function mutants of the JIL-1 histone H3S10 kinase. *Genetics* **177,** 79-87.

Deng, H., Bao, X., Cai, W., Blacketer, M.J., Belmont, A.S., Girton, J., Johansen, J., and Johansen, K.M. (2008). Ectopic histone H3S10 phosphorylation causes chromatin structure remodeling in *Drosophila. Development* **135,** 699-705.

Girton, J., Wang, C., Johansen, J., and Johansen, K.M. (2013). The effect of *JIL-1* on position-effect variegation is proportional to the total amount of heterochromatin in the genome. *Fly* **7,** 129-133.

Gong, W.J. and Golic, K.G. (2004). Genomic deletions of the *Drosophila melanogaster* Hsp70 genes. *Genetics* **168,** 1467-1476.

Gruenbaum Y, Landesman Y, Drees B, Bare JW, Saumweber H, Paddy, M.R., Sedat, J.W., Smith, D.E., Benton, B.M., and Fisher, P. (1988). *Drosophila* nuclear lamin precursor Dm0 is translated from either of two developmentally regulated mRNA species apparently encoded by a single gene. *J. Cell Biol.* **106,** 585-596.

Ivaldi, M.S., Karam, C.S., and Corces, V.G. (2007). Phosphorylation of histone H3 at Ser10 facilitates RNA polymerase II release from promoter-proximal pausing in *Drosophila*. *Genes Dev.* **21,** 2818-2831.

Ji, Y., Rath, U., Girton, J., Johansen, K.M., and Johansen, J. (2005). D-Hillarin, a novel W180-domain protein, affects cytokinesis through interaction with the septin family member Pnut. *J. Neurobiol.* **64,** 157-169.

Ji, Y., and Tulin, A.V. (2009). Poly(ADP-ribosyl)ation of heterogeneous nuclear ribonucleoproteins modulates splicing. *Nucleic Acids Res.* **37,** 3501-3513

Jin, Y., Wang, Y., Walker, D.L, Dong, H., Conley, C., Johansen, J., and Johansen, K.M. (1999). JIL-1: a novel chromosomal tandem kinase implicated in transcriptional regulation in *Drosophila*. *Mol. Cell* **4,** 129-135.

Jin, Y., Wang, Y., Johansen, J., and Johansen, K.M. (2000). JIL-1, a chromosomal kinase implicated in regulation of chromatin structure, associates with the MSL dosage compensation complex. *J. Cell Biol.* **149,** 1005-1010.

Johansen, K.M., and Johansen, J. (2003). Studying nuclear organization in embryos using antibody tools. In *Drosophila Cytogenetics Protocols.* D.S. Henderson, Ed., Humana Press, Totowa, New Jersey. p. 215-234.

Johansen, K.M., Cai, W., Deng, H., Bao, X., Zhang, W., Girton, J., and Johansen, J. (2009). Methods for studying transcription and epigenetic chromatin modification in *Drosophila* polytene chromosome squash preparations using antibodies. *Methods* **48,** 387-397.

Kotova, E., Jarnik, M., and Tulin, A.V. (2010). Uncoupling of the transactivation and transrepression functions of PARP1 protein. *Proc. Natl. Acad. Sci. USA* **107,** 6406-6411.

Lake, C.M., Holsclaw, J.K., Bellendir, S.P., Sekelsky, J., and Hawley, R.S. (2013). The development of a monoclonal antibody recognizing the *Drosophila melanogaster* phosphorylated histone H2A variant (γ-H2AV). *G3: Genes Genom. Genet.* **3,**1539-1543.

Lerach, S., Zhang, W., Deng, H., Bao, X., Girton, J., Johansen, J., and Johansen, K.M. (2005). JIL-1 kinase, a member of the male-specific lethal (MSL) complex, is necessary for proper dosage compensation of eye pigmentation in *Drosophila*. *Genesis* **43,** 213-215.

Lerach, S., Zhang, W., Bao, X., Deng, H., Girton, J., Johansen, J., and Johansen, K.M. (2006). Loss-of-function alleles of the JIL-1 kinase are strong suppressors of position

effect variegation of the w^{m4} allele in Drosophila. *Genetics* **173,** 2403-2406.

Li, Y., Cai, W., Wang, C., Deng, H., Bao, X., Zhang, W., Girton, J., Johansen, J., and Johansen, K.M. (2012). The Mof acetyltransferase is required for JIL-1 H3S10ph kinase stability in *Drosophila* males. *Mol. Biol. Cell* **23,** 734. doi:10.1091/mbc.E12-10-0757.

Li, Y., Cai, W., Wang, C., Yao, C., Bao, X., Deng, H., Girton, J., Johansen, J., and Johansen, K.M. (2013). Domain requirements of the JIL-1 tandem kinase for histone H3 serine10 phosphorylation and chromatin remodeling *in vivo*. *J. Biol. Chem.* **288,** 19441-19449.

Lindsley, D.L., and Zimm, G.G. (1992). *The genome of Drosophila melanogaster*. Academic Press, New York, NY.

Madigan, J.P., Chotkowski, H.L., and Glaser, R.L. (2002). DNA double-strand break-induced phosphorylation of *Drosophila* histone variant H2Av helps prevent radiation-induced apoptosis. *Nucleic Acids Res.* **30,** 3698-3705.

Mohamed, M.F., and Hollfelder, F. (2012). Efficient crosswise catalytic promiscuity among enzymes that catalyze phosphoryl transfer. *Biochem. Biophys. Acta* **1834,** 417-424.

Nowak, S.J., Pai, C.-Y., and Corces, V.G. (2003). Protein phosphatase 2A activity affects histone H3 phosphorylation and transcription in *Drosophila melanogaster*. *Mol. Cell Biol.* **23,** 6129-6138.

Peck, S.C. (2006). Analysis of protein phosphorylation: methods and strategies for studying kinases and substrates. Plant. J. *45,* 512-522.

Regnard, C., Straub, T., Mitterweger, A., Dahlsveen, I.K., Fabian, V., and Becker, P. (2011). Global analysis of the relationship between JIL-1 kinase and transcription. *PLoS Genetics* **7,** e1001327.

Roberts, D.B. (1998). In *Drosophila: A Practical Approach* IRL Press, Oxford, UK.

Sambrook, J., and Russell, D. W. (2001). Molecular Cloning: A Laboratory Manual. Cold Spring Harbor Laboratory Press, NY.

Swaminathan, J., Baxter, E.M., and Corces, V.G. (2005). The role of histone H2Av variant replacement and histone H4 acetylation in the establishment of Drosophila heterochromatin. *Genes Dev.* **19,** 844-858.

Thomas, C.J., Kotova, E., Andrake, M., Adolf-Bryfolgle, J., Glaser, R., Regnard, C., and Tulin, A.V. (2014). Kinase-mediated changes in nucleosome conformation trigger chromatin decondensation via poly(ADP-rybosyl)ation. *Mol. Cell* **53,** 831-842.

Tulin, A., Stewart, D., and Spradling, A.C. (2002). The Drosophila heterochromatic gene encoding poly(APD-ribose) polymerase (PARP) is required to modulate chromatin structure during development. *Genes Dev.* **16,** 2108-2119.

Van Daal, A., and Elgin, S.C.R. (1992). A histone H2A variant, H2AvD, is essential in *Drosophila melanogaster*. *Mol. Biol. Cell* **3,** 593-602.

Wang, C., Girton, J., Johansen, J., and Johansen, K.M. (2011a). A balance between euchromatic (JIL-1) and heterochromatic (SU(VAR)2-5 and SU(VAR)3-9) factors regulates position-effect variegation in Drosophila. *Genetics* **188,** 745-748.

Wang, C., Cai, W., Li, Y., Deng, H., Bao, X., Girton, J., Johansen, J., and Johansen, K.M. (2011b). The epigenetic H3S10 phosphorylation mark is required for counteracting heterochromatic spreading and gene silencing in *Drosophila melanogaster*. *J. Cell Sci.* **124,** 4309-4317.

Wang, C., Cai, W., Li, Y., Girton, J., Johansen, J., and Johansen, K.M. (2012). H3S10 phosphorylation by the JIL-1 kinase regulates H3K9 dimethylation and gene expression at the *white* locus in *Drosophila.* *Fly* **6,** 1-5.

Wang, C., Yao, C., Li, Y., Cai, W., Bao, X., Girton, J., Johansen, J., and Johansen, K.M. (2013). Evidence against a role for the JIL-1 kinase in H3S28 phosphorylation and 14-3-3 recruitment to active genes in *Drosophila*. *PLoS ONE* **8,** e62484.

Wang, Y., Zhang, W., Jin, Y., Johansen, J., and Johansen, K.M. (2001). The JIL-1 tandem kinase mediates histone H3 phosphorylation and is required for maintenance of chromatin structure in *Drosophila*. *Cell* **105,** 433-443.

Weeks, J.R., Hardin, S.E., Shen, J., Lee, J.M., and Greenleaf, A.L. (1993). Locus-specific variation in phoshorylation state of RNA polymerase II in vivo: correlations with gene activity and transcript processing. *Genes Dev.* **7,** 2329-2344.

Xue, L., Wang, W-H., Iliuk, A., Hu, L., Galan, J.A., Yu, S., Hans, M., Geahlen, R.L., and Tao, W.A. (2012). Sensitive kinase assay linked with phosphoproteomics for identifying direct kinase substrates. *Proc. Natl. Acad. Sci. USA* **109,** 5615-5620.

Zhang, W., Jin, Y., Ji, Y., Girton, J., Johansen, J., and Johansen, K.M. (2003). Genetic and phenotypic analysis of alleles of the *Drosophila* chromosomal JIL-1 kinase reveals a functional requirement at multiple developmental stages. *Genetics* **165,** 1341-1354.

Zhang, W., Deng, H., Bao, X., Lerach, S., Girton, J., Johansen, J., and Johansen, K.M. (2006). The JIL-1 histone H3S10 kinase regulates dimethyl H3K9 modifications and heterochromatic spreading in *Drosophila*. *Development* **133***,* 229-235.

Figures

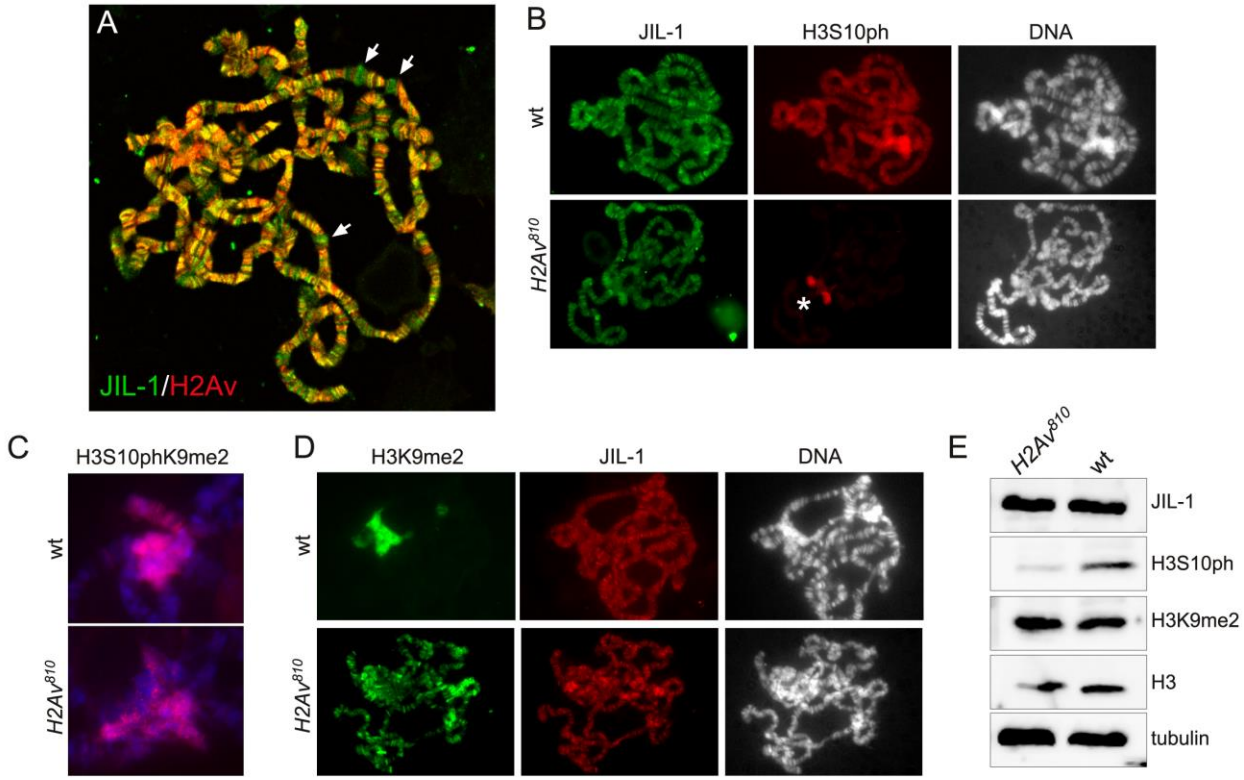

Figure 1. Immunocytochemical and immunoblot characterization of JIL-1, H3S10ph, and H3K9me2 in wild type and *H2Av* null mutant backgrounds. (A) Confocal image of a polytene squash preparation double labeled with antibodies to JIL-1 (in green) and H2Av (in red). While largely co-localized as indicated by the yellow/orange coloring, many interband locations were only positive for either JIL-1 (arrows) or H2Av. (B) Polytene squash preparations from wildtype and homozygous *H2Av*^{810} null larvae double labeled with antibodies to JIL-1 (in green) and H3S10ph (in red). The asterisk indicates H3S10ph labeling at the chromocenter in the *H2Av*^{810} null mutant background. DNA labeling by Hoechst is shown in grey. (C) Chromocenters from polytene squash preparations from wildtype and homozygous *H2Av*^{810} null larvae labeled with antibody to the H3S10phK9me2 double mark (in red). DNA labeling by Hoechst is shown in blue. (D) Polytene squash preparations from wild-type and homozygous *H2Av*^{810} null mutant

larvae double labeled with antibodies to H3K9me2 (in green) and JIL-1 (in red). DNA labeling by Hoechst is shown in grey. (E) Immunoblots of protein extracts from salivary glands from wild-type and homozygous *H2Av*^{810} null larvae labeled with antibodies to JIL-1, H3S10ph, and H3K9me2. Labeling with histone H3 and tubulin antibody was used as loading controls.

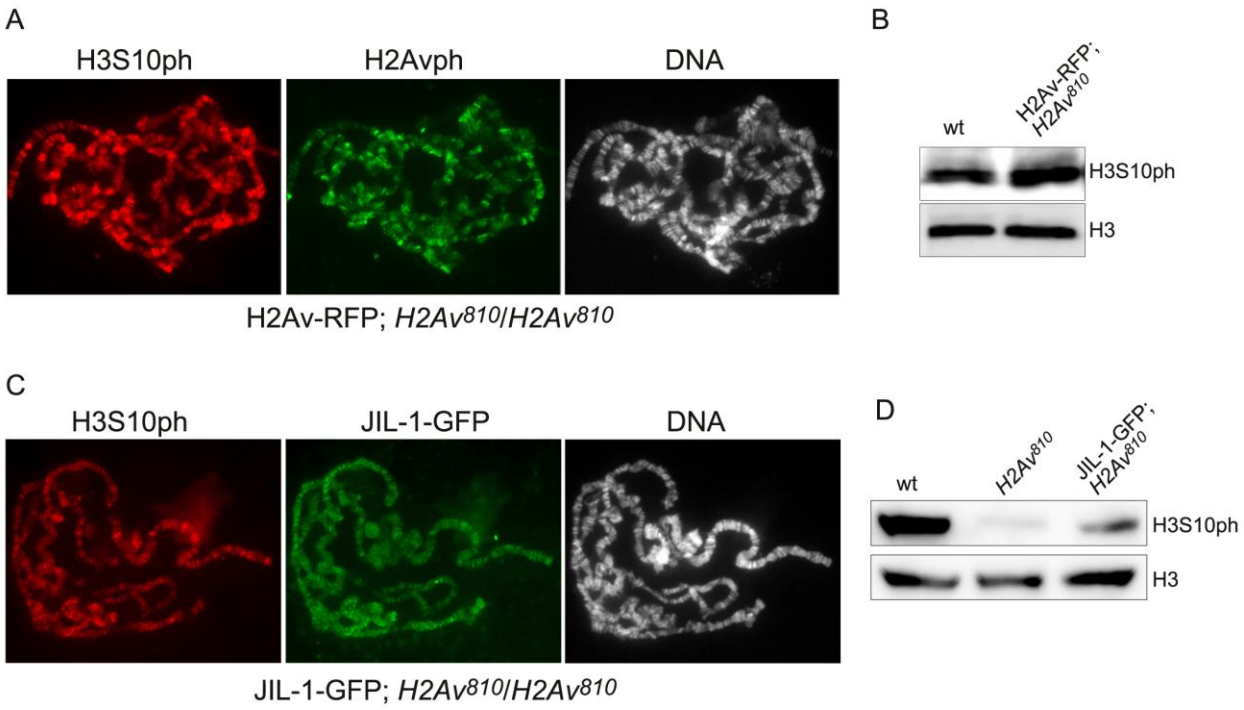

Figure 2. Immunocytochemical and immunoblot analysis of *H2Av-RFP* and *JIL-1-GFP* transgene expression in the *H2Av* null mutant background. (A) Polytene squash preparation from a homozygous *H2Av*^{810} null larvae expressing the *H2Av-RFP* transgene double labeled with antibodies to H3S10ph (in red) and H2Avph (in green). DNA labeling by Hoechst is shown in grey. (B) Immunoblots of protein extracts from salivary glands from a wild type and a homozygous *H2Av*^{810} null larvae expressing the *H2Av-RFP* transgene labeled with antibody to H3S10ph. Labeling with histone H3 antibody was used as a loading control. (C) Polytene squash preparation from a homozygous *H2Av*^{810} null larvae expressing the *JIL-1-GFP* transgene double labeled with antibodies to H3S10ph (in red) and GFP (in green). DNA labeling by Hoechst is shown in grey. (D) Immunoblots of protein extracts from salivary glands from a wild type, a homozygous *H2Av*^{810} null, and a homozygous *H2Av*^{810} null larvae expressing the *JIL-1-GFP* transgene labeled with antibody to H3S10ph. Labeling with tubulin antibody was used as a loading control.

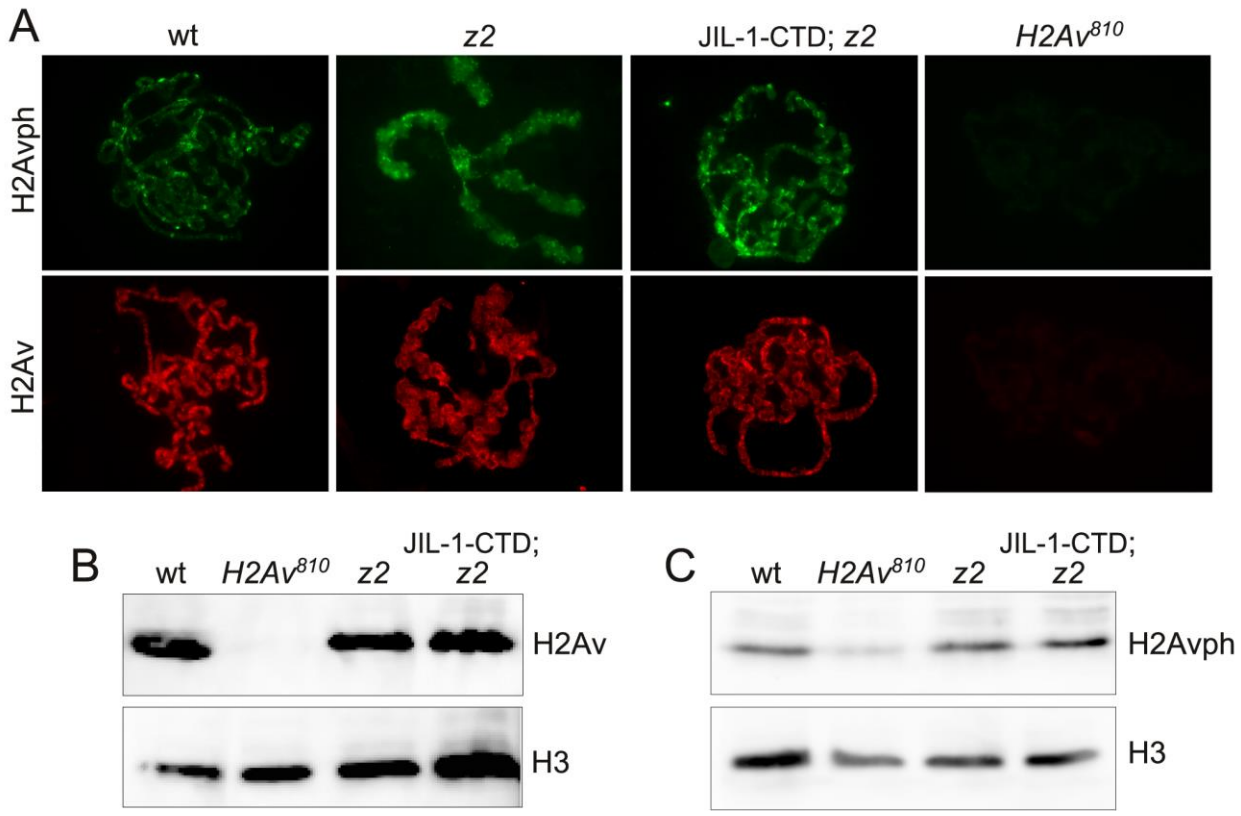

Figure 3. Immunocytochemical and immunoblot analysis of H2Av and H2Avph in the *JIL-1* null mutant background. (A) Polytene squash preparation from wild-type (wt), homozygous *JIL-1*^{z2} null (*z2*), homozygous *JIL-1*^{z2} null expressing the CFP-tagged JIL-1-CTD transgene (JIL-1-CTD; *z2*), and homozygous *H2Av*^{810} null larvae labeled with antibodies to H2Avph (in green) and H2Av (in red), respectively. (B) Immunoblots of protein extracts from salivary glands from wild-type (wt), homozygous *H2Av*^{810} null, homozygous *JIL-1*^{z2} null (*z2*), and homozygous *JIL-1*^{z2} null larvae expressing the CFP-tagged JIL-1-CTD transgene (JIL-1-CTD; *z2*) labeled with antibody to H2Av. Labeling with histone H3 antibody was used as a loading control. (C) Immunoblots of protein extracts from salivary glands from wild-type (wt), homozygous *H2Av*^{810} null, homozygous *JIL-1*^{z2} null (*z2*), and homozygous *JIL-1*^{z2} null larvae expressing the CFP-tagged

JIL-1-CTD transgene (JIL-1-CTD; *z2*) labeled with antibody to H2Avph. Labeling with histone H3 antibody was used as a loading control.

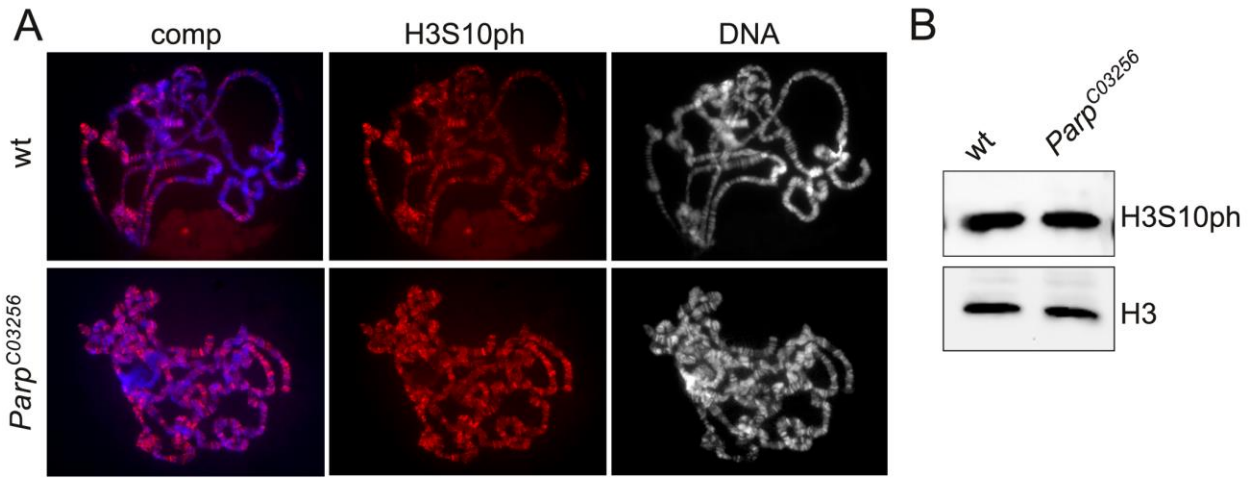

Figure 4. Decreased levels of PARP-1 activity do not affect H3S10 phosphorylation by JIL-1. (A) Polytene squash preparations from wild-type (wt) and hypomorphic homozygous *Parp*^{C03256} mutant larvae labeled with antibody to H3S10ph (in red) and with Hoechst (DNA in blue/grey). Immunoblots of protein extracts from salivary glands from wild-type (wt), and hypomorphic homozygous *Parp*^{C03256} mutant larvae labeled with antibody to H3S10ph. Labeling with histone H3 antibody was used as a loading control.

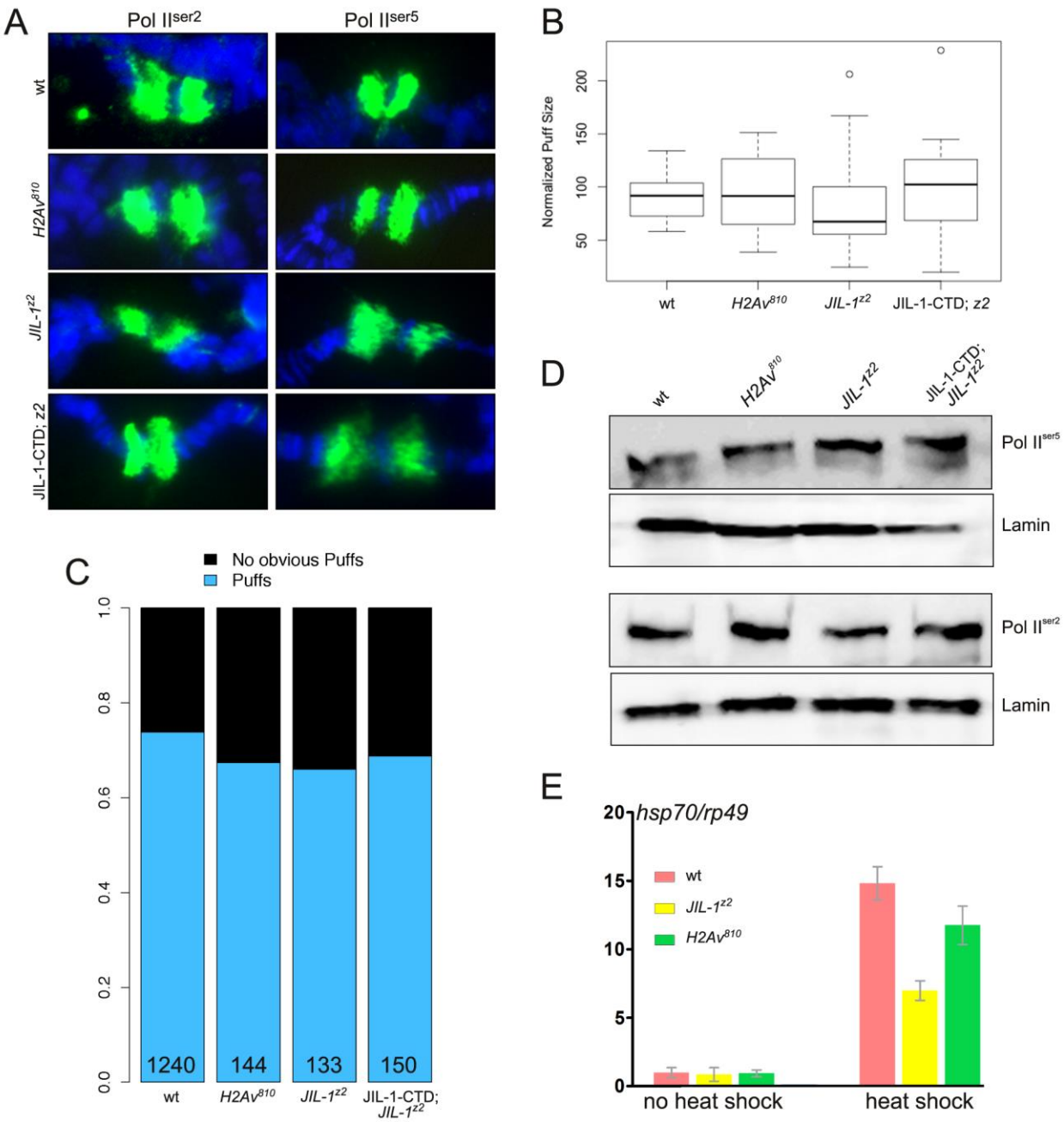

Figure 5. Neither JIL-1 nor H2Av is required for chromatin decondensation or transcriptional elongation during heat shock. (A) 87 A/C heat shock puffs from polytene squash preparations labeled with Pol II0^{ser2} and Pol II0^{ser5} antibody from wild-type (wt), homozygous *H2Av*^{810} null, homozygous *JIL-1*^{z2} null (*z2*), and homozygous *JIL-1*^{z2} null larvae

expressing the CFP-tagged JIL-1-CTD transgene (JIL-1-CTD; *z2*). (B) Box plot of normalized 87 A/C puff size from wild-type (wt), homozygous *H2Av*^{810} null, homozygous *JIL-1*^{z2} null (*z2*), and homozygous *JIL-1*^{z2} null larvae expressing the CFP-tagged JIL-1-CTD transgene (JIL-1-CTD; *z2*). Measurements were obtained from more than 30 salivary gland nuclei from at least five different larvae for each genotype. The box plot representation defines 25th to 75th percentiles (boxes), 50th percentile (lines in boxes), and ranges (whiskers, 1.5 times the interquartile range extended from both ends of the box or the maximal/minimal value). There was no statistically significant difference in puff size between the four genotypes (P>0.15; ANOVA test). (C) Stack bar charts showing the distribution of salivary gland nuclei with clearly recognizable puffs among the total number of nuclei examined from wildtype (wt), homozygous *H2Av*^{810} null, homozygous *JIL-1*^{z2} null (*z2*), and homozygous *JIL-1*^{z2} null larvae expressing the CFP-tagged JIL-1-CTD transgene (JIL-1-CTD; *z2*). The total number of nuclei examined is indicated for each genotype. (D) Immunoblots of protein extracts labeled with Pol II0^{ser2} and Pol II0^{ser5} antibody from wild-type (wt), homozygous *H2Av*^{810} null, homozygous *JIL-1*^{z2} null (*z2*), and homozygous *JIL-1*^{z2} null larvae expressing the CFP-tagged JIL-1-CTD transgene (JIL-1-CTD; *z2*). Labeling with lamin antibody was used as a loading control. (E) Transcript levels of *hsp70* mRNA in wild-type (wt) and homozygous *H2Av*^{810} and *JIL-1*^{z2} null mutant backgrounds in response to heat shock treatment. *hsp70* transcript levels were determined by qRT-PCR and normalized to the mRNA levels of the control non-heat shock protein Rp49 (ribosomal protein 49) both without and after heat shock treatment. The data shown are the average from three independent experiments where each determination of transcript levels was performed in duplicate. The error bars indicate the SDM.

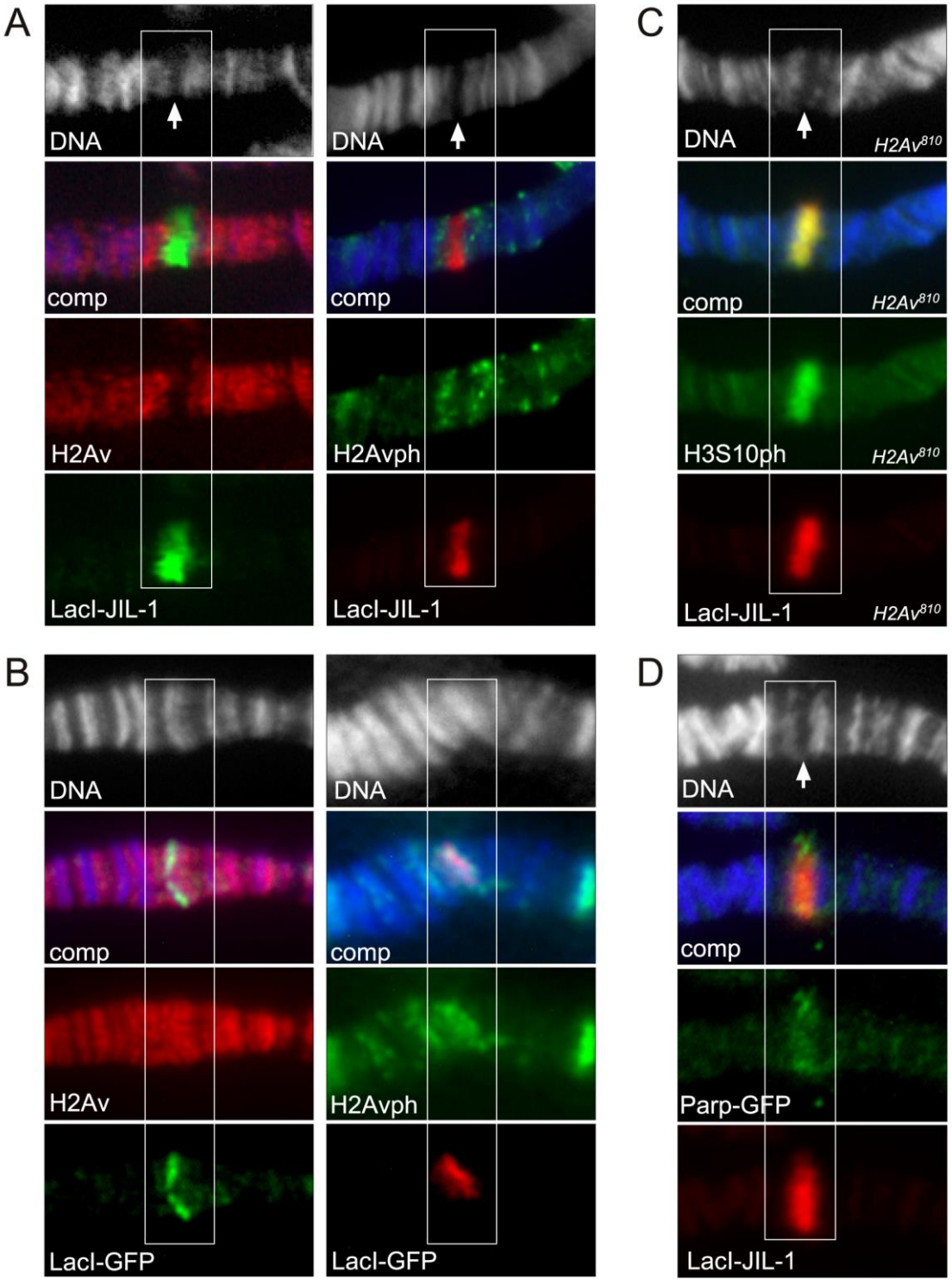

Figure 6. Tethering of LacI-tagged JIL-1 constructs to a polytene chromosome band *LacO* insertion site. The panels show antibody/Hoechst labelings of polytene squash preparations from third instar larvae homozygous for the *lacO* repeat line *P11.3* which is inserted into the middle of a polytene band in region 96C1-2. (A) Tethering of full-length LacI-JIL-1. The white boxes indicate the location of the polytene band with the *lacO* repeat insertion site. The white arrows indicate the "split" in the polytene bands reflecting decondensation of the chromatin when LacI-JIL-1 is tethered to the band. The LacI-tagged constructs were detected with anti-LacI antibody, H2Av with anti-H2Av antibody, and H2Avph with anti-H2Avph antibody. DNA was labeled with Hoechst (in blue/grey). (B) Tethering of LacI-GFP. The white boxes indicate the location of the polytene band with the *lacO* repeat insertion site. In contrast to when LacI-JIL-1 is tethered there is no opening of the band. The LacI-tagged constructs were detected with anti-LacI antibody, H2Av with anti-H2Av antibody, and H2Avph with anti-H2Avph antibody. DNA was labeled with Hoechst (in blue/grey). (C) Tethering of full-length LacI-JIL-1 in a homozygous $H2Av^{810}$ null mutant background. The white box indicates the location of the polytene band with the *lacO* repeat insertion site. The white arrow indicates the "split" in the polytene bands reflecting decondensation of the chromatin when LacI-JIL-1 is tethered to the band. The LacI-JIL-1 was detected with anti-LacI antibody and H3S10ph with anti-H3S10ph antibody. DNA was labeled with Hoechst (in blue/grey). (D) Tethering of full-length LacI-JIL-1 from a preparation co-expressing GFP-tagged PARP-1 (Parp-GFP). The white box indicates the location of the polytene band with the *lacO* repeat insertion site. The white arrow indicates the "split" in the polytene bands reflecting decondensation of the chromatin when LacI-JIL-1 is tethered to the band. The LacI-JIL-1 was detected with anti-LacI antibody and Parp-GFP with anti-GFP antibody. DNA was labeled with Hoechst (in blue/grey).

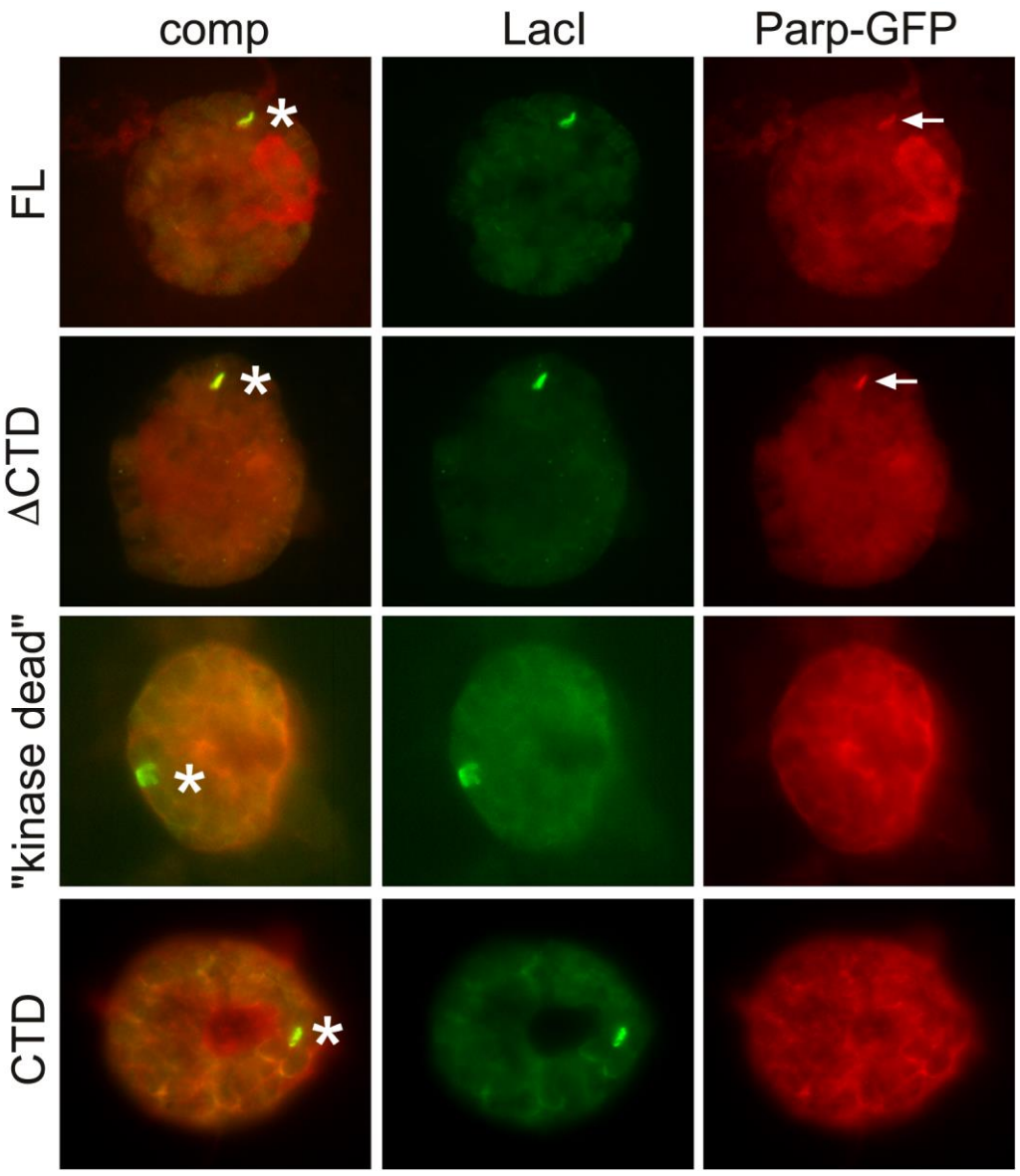

Figure 7. Tethering of LacI-tagged JIL-1 constructs to a polytene chromosome band *LacO* insertion site. The panels show antibody labelings of smush preparations from third instar larvae homozygous for the *lacO* repeat line *P11.3* which is inserted into the middle of a polytene band in region 96C1-2. The figure shows mush preparations in which full-length LacI-JIL-1 (FL), LacI-JIl-1- ΔCTD (ΔCTD), LacI-JIL-1-"kinase dead" ("kinase dead"), and LacI-JIL-1-CTD (CTD) were tethered to the *lacO* repeats, respectively, in nuclei co-expressing Parp-GFP. LacI-tagged

constructs were detected with anti-LacI antibody and Parp-GFP with anti-GFP antibody. Asterisks indicate the *lacO* repeat insertion sites. Arrows point to enhanced recruitment of Parp-GFP to the insertion sites when LacI-JIL-1 constructs with intact H3S10 phosphorylation activity are tethered (e.g. FL and ΔCTD).